JACS
JOURNAL OF THE AMERICAN CHEMICAL SOCIETY
Communication
pubs.acs.org/JACS

Anomalous High Ionic Conductivity of Nanoporous β-Li_3PS_4

Zengcai Liu,[†] Wujun Fu,[†] E. Andrew Payzant,[†,‡] Xiang Yu,[†] Zili Wu,[†,§] Nancy J. Dudney,[‡] Jim Kiggans,[‡] Kunlun Hong,[†] Adam J. Rondinone,[†] and Chengdu Liang*[,†]

[†]Center for Nanophase Materials Sciences, Oak Ridge National Laboratory, Oak Ridge, Tennessee 37830, United States
[‡]Materials Science and Technology Division, Oak Ridge National Laboratory, Oak Ridge, Tennessee 37830, United States
[§]Chemical Sciences Division, Oak Ridge National Laboratory, Oak Ridge, Tennessee 37830, United States

Supporting Information

ABSTRACT: Lithium-ion-conducting solid electrolytes hold promise for enabling high-energy battery chemistries and circumventing safety issues of conventional lithium batteries. Achieving the combination of high ionic conductivity and a broad electrochemical window in solid electrolytes is a grand challenge for the synthesis of battery materials. Herein we show an enhancement of the room-temperature lithium-ion conductivity by 3 orders of magnitude through the creation of nanostructured Li_3PS_4. This material has a wide electrochemical window (5 V) and superior chemical stability against lithium metal. The nanoporous structure of Li_3PS_4 reconciles two vital effects that enhance the ionic conductivity: (1) the reduction of the dimensions to a nanometer-sized framework stabilizes the high-conduction β phase that occurs at elevated temperatures, and (2) the high surface-to-bulk ratio of nanoporous β-Li_3PS_4 promotes surface conduction. Manipulating the ionic conductivity of solid electrolytes has far-reaching implications for materials design and synthesis in a broad range of applications, including batteries, fuel cells, sensors, photovoltaic systems, and so forth.

The paradigm shift from small power sources of personal electronics to large-scale energy storage devices for electric vehicles and electricity grids poses grand challenges to the storage of electricity at high density with enhanced safety requirements.[1−7] Although promising, the current lithium-ion batteries that use organic liquids as electrolytes have many limitations for achieving high energy density. For example, lithium metal, which has the highest gravimetric energy density of all anode materials, cannot be used with a liquid electrolyte because of the compromised cyclability and concerned safety issues. Replacing organic liquid electrolytes with solid electrolytes would bring a new perspective to research on lithium-ion batteries, enabling high-energy battery chemistry with an intrinsically safe cell design.[2] Nevertheless, solid electrolytes have not been widely used in lithium-ion batteries because their ionic conductivities are generally too low to meet the required current density. Many of the lithium-ion-conducting materials have good compatibility with lithium metal, but their conductivities are still a few orders of magnitude lower than that of the liquid electrolytes. In addition, high interfacial resistance is a challenge for solid electrolytes.

Lithium thiophosphates have been intensively studied as promising solid electrolytes for all-solid lithium batteries. Although the ionic conductivity of lithium thiophosphates can be optimized to achieve values as high as 3×10^{-3} S cm^{-1},[8] these metastable materials require stringent synthesis conditions such as long-time, low-energy ball milling and quenching. A recent report showed that the partial substitution of P atoms by Ge atoms in the lithium thiophosphate forms $Li_{10}GeP_2S_{12}$, which has an unprecedented high ionic conductivity of 1.2×10^{-2} S cm^{-1}, a value comparable to those of the liquid electrolytes used in lithium-ion batteries. Unfortunately, the Ge atoms in the structure compromise the chemical compatibility of the lithium thiophosphate with lithium metal,[9] and therefore, indium metal is used as anode in the batteries. While the pursuit of high ionic conductivity through innovative chemical structures remains as the momentum for novel lithium-ion conductors, we demonstrate herein that creating nanostructures of existing lithium thiophosphate materials can be another route to achieve improvement of the ionic conductivity in solid electrolytes by several orders of magnitude with the advantage of not interrupting their chemical stabilities. To the best or our knowledge, this is first report of nanostructured lithium thiophosphate.

Li_3PS_4 is the most stable chemical in the Li_2S−P_2S_5 system. Bulk Li_3PS_4 is a γ phase that has a low ionic conductivity of 3×10^{-7} S cm^{-1} at room temperature (line c in Figure 1).[4,10] When heated to 195 °C, γ-Li_3PS_4 is converted to the high-conduction β-Li_3PS_4 phase (line b in Figure 1; the nomenclature for Li_3PS_4 was adopted from ref 4), which shows an abrupt increase of ionic conductivity in the Arrhenius plot.[4,10] The high-conduction β phase reverts back to the γ phase at temperatures below 195 °C. Extrapolation of lines b and c in Figure 1 gives conductivities of 8.93×10^{-7} and 2.61×10^{-7} S cm^{-1} for the β and γ phases, respectively, at 25 °C. In striking contrast, nanoporous Li_3PS_4 synthesized by a wet-chemical method gives an anomalous room-temperature ionic conductivity of 1.6×10^{-4} S cm^{-1}, which is nearly 3 orders of magnitude higher than that of crystalline Li_3PS_4.[10] Line a in Figure 1 shows a continuous linear relationship between the conductivity of the nanoporous Li_3PS_4 and the reciprocal of the absolute temperature ($1/T$) over the temperature range from −20 to 100 °C.

Received: November 12, 2012
Published: January 10, 2013

dx.doi.org/10.1021/ja3110895 | J. Am. Chem. Soc. 2013, 135, 975−978

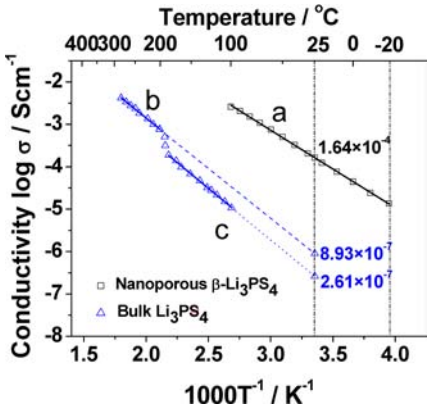

Figure 1. Arrhenius plots for nanoporous β-Li_3PS_4 (line a), bulk β-Li_3PS_4 (line b), and bulk γ-Li_3PS_4 (line c). The conductivity data for bulk Li_3PS_4 are reproduced from the work of Tachez.[10].

Decomposition of Li_3PS_4·3THF forms β-Li_3PS_4. Conventionally, Li_3PS_4 has been synthesized through the solid-state reaction of Li_2S with P_2S_5 at 520 °C,[4,10,11] which affords nonporous crystals of Li_3PS_4. In this research, we found that the reaction of Li_2S and P_2S_5 can be mediated by tetrahydrofuran (THF) at room temperature (eq 1). Elemental analysis gave a stoichiometric composition of Li_3PS_4·3THF for the as-synthesized powder. The removal of THF affords pure Li_3PS_4.

$$Li_2S + P_2S_5 \xrightarrow{THF} Li_3PS_4\cdot 3THF \quad (1)$$

The as-synthesized powder is well-crystallized with a strong X-ray diffraction (XRD) peak at $2\theta \approx 8.4°$ and other diffraction peaks with significantly lower intensity (Figure 2a). The shift of the lowest diffraction peak of pure Li_3PS_4 at $2\theta = 13.6°$ to $2\theta = 8.4°$ for the as-synthesized powder is an indication that the as-synthesized sample contains cocrystallized THF molecules. The Raman spectrum (Figure S1 in the Supporting Information) shows the characteristic $\nu_s(PS_4)$ peak at 422 cm^{-1}, which is in good agreement with that for pure Li_3PS_4.[10,12] The C−H vibrations of THF are clearly identified by the peaks at 2850−3050 cm^{-1} in the Raman spectrum.[13] Additional peaks at lower frequencies indicate the strong coordination of the oxygen in THF with the lithium ions in Li_3PS_4. Thermogravimetric analysis (TGA) showed that the THF molecules can be readily removed at temperatures below 80 °C. The weight loss obtained from the TGA curve (Figure 2b) agrees with the chemical composition of Li_3PS_4·3THF measured by elemental analysis. The forward scan of differential scanning calorimetry (DSC) for Li_3PS_4·3THF in the first cycle has a large endothermic peak with an onset temperature at 50 °C and a small exothermic peak with an onset at 140 °C. The endothermic peak corresponds to the dissociation of THF, and the exothermic peak is related to the crystallization of Li_3PS_4. It is interesting that the reverse scan of the first DSC cycle has no peaks. This observation indicates that the dissociation of THF and crystallization of Li_3PS_4 are irreversible over the temperature range from 25 to 350 °C. No phase transition was observed in the second DSC cycle. When heated at 80 °C, crystalline Li_3PS_4·3THF decomposes to form amorphous Li_3PS_4, as evidenced by the featureless XRD pattern in Figure 2a and the characteristic $\nu_s(PS_4)$ Raman peak at 422 cm^{-1} in Figure S1. Further heating to 140 °C yields crystalline β-Li_3PS_4 (Figure 2a). The DSC scan (Figure 2b)

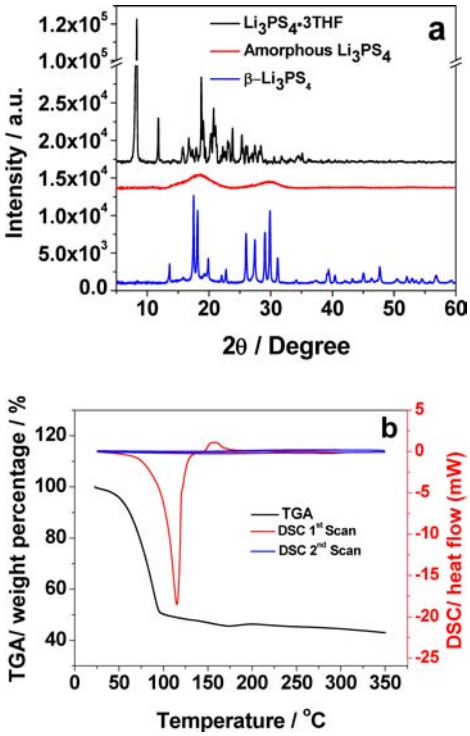

Figure 2. Structural evolution of β-Li_3PS_4. (a) XRD patterns of as-synthesized Li_3PS_4·3THF, amorphous Li_3PS_4 prepared by heating Li_3PS_4·3THF at 80 °C, and nanoporous β-Li_3PS_4 prepared by heating Li_3PS_4·3THF at 140 °C. (b) Thermal analysis for the as-synthesized powder. The black line is the TGA curve at 10 °C/min under N_2. The red and blue lines are the first and second DSC cycles from room temperature to 350 °C.

confirmed that the β phase is stable over a broad temperature range from room temperature to 350 °C.

Nanostructure stabilizes the metastable β-Li_3PS_4. It is well-documented that β-Li_3PS_4 is a metastable phase that occurs at elevated temperatures and transforms to the more stable γ-Li_3PS_4 at temperatures below 195 °C.[4] Why then does the wet-chemically synthesized β-Li_3PS_4 exist over a broad temperature range? A close examination of the material revealed that a subtle nanostructure evolved during the removal of solvent. The micrograph in Figure 3a shows the as-synthesized Li_3PS_4·3THF powder, which has an orthorhombic morphology sized between 10 and 30 μm. The Li_3PS_4·3THF powder has no measurable surface area as determined by nitrogen adsorption (Figure 3d). Heating at 140 °C results in a 54% weight loss due to the removal of THF; however, both the morphology and the size of the original Li_3PS_4·3THF particles are preserved (Figure 3b). The high-resolution micrograph of the Li_3PS_4 after heating (Figure 3c) reveals a highly porous structure. Significant nitrogen adsorption occurs at relative pressures above 0.9 in the isotherm of Figure 3d. This material has a Brunauer−Emmett−Teller (BET) surface area of 15.6 m^2 g^{-1}. The Figure 3d inset shows a plot of the pore size distribution of β-Li_3PS_4. The average pore size from the BET measurement is about 28 nm, which is consistent with pore size estimated by small-angle XRD measurements (Figure S2). The framework of the porous β-Li_3PS_4 has an average size of 80−100 nm, as calculated from the peak width of the powder XRD pattern and estimated from the micrograph (Figure 3c). The surface energy of the Li_3PS_4 is significantly increased when a nanoporous structure is developed. The high surface energy could induce a chemical

dx.doi.org/10.1021/ja3110895 | J. Am. Chem. Soc. 2013, 135, 975−978

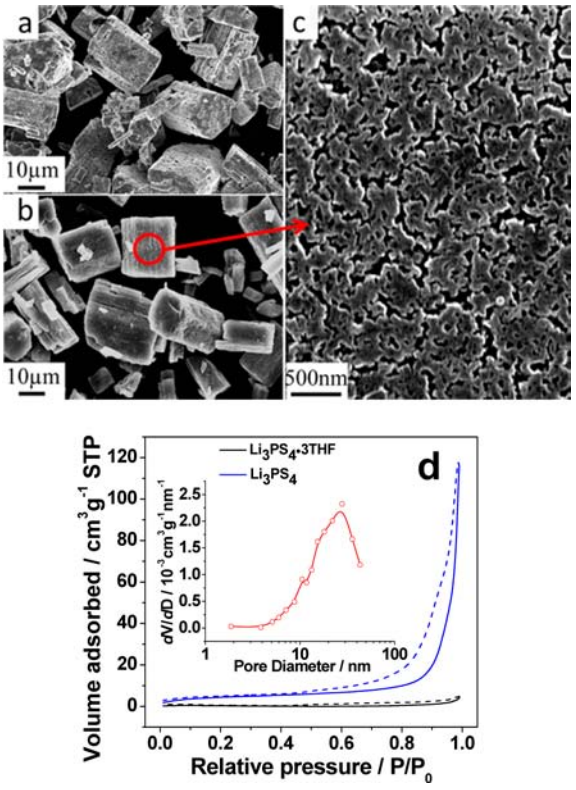

Figure 3. Characterization of the porous structure. (a) Morphology of as-synthesized Li_3PS_4·3THF particles. (b) Morphology of nanoporous β-Li_3PS_4 particles. (c) Surface of the nanoporous β-Li_3PS_4. (d) N_2 adsorption/desorption isotherms at 77 K. The inset shows the pore size distribution of β-Li_3PS_4 calculated using the adsorption branch of the isotherm.

lattice distortion that downshifts the phase transition temperature.[14] This phenomenon is akin to the stabilization of α-AgI by reducing the particle size to the nanometer range.[1,15,16] It is reasonable to conclude that the fine nanoporous framework stabilizes the metastable β-Li_3PS_4 over a broad temperature range. Compared with γ-Li_3PS_4, β-Li_3PS_4 is expected to be a high-conduction phase because of the large interstitials that facilitate the movement of lithium ions (Figure S3).

Surface conduction boosts the overall conductivity of nanoporous β-Li_3PS_4. The ionic conductivity of nanoporous β-Li_3PS_4 was measured to be 1.6×10^{-4} S cm^{-1} at 25 °C, which is much higher than the intrinsic ionic conductivity of 8.93×10^{-7} S cm^{-1} for bulk β-Li_3PS_4 derived by extrapolating line b in Figure 1. The calculated activation energy for the nanoporous β-Li_3PS_4 is 0.356 eV, which is 0.114 eV lower than that of the bulk β-Li_3PS_4 (0.47 eV[10]). Obviously, there must be a different ionic conduction mechanism that contributes to the high conductivity of the nanoporous β-Li_3PS_4. To unravel the origin of the high ionic conductivity of the nanoporous β-Li_3PS_4, representative samples with varying crystallinity and surface area were investigated through heat treatments from 80 to 200 °C (Figure 4). After the removal of THF at 80 °C, the amorphous Li_3PS_4 has a high surface area of 40 m^2 g^{-1} and a low ionic conductivity of 7.4×10^{-5} S cm^{-1}. Heating the amorphous Li_3PS_4 toward the crystallization temperature at 140 °C diminishes the surface area, while the ionic conductivity is dramatically increased. Therefore, the transition from amorphous to crystalline β-Li_3PS_4 is critical for high ionic conductivity. Further heating of the material to 200 °C leads

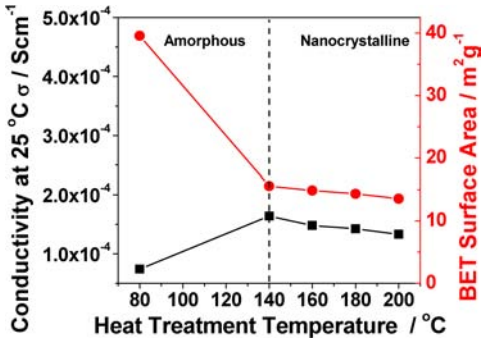

Figure 4. Correlation of room-temperature ionic conductivity to the surface area and crystallinity of samples thermally treated from 80 to 200 °C.

to a progressive decline in surface area. The total ionic conductivity follows the trend of surface area change with heat treatment. In other words, the ionic conductivity of nanoporous β-Li_3PS_4 has a positive correlation with the surface area of the material.

Rietveld refinement analysis revealed that the peak broadening originates from the microstrain and the size effect of the fine framework of the nanoporous material (Figure S4). Nonetheless, no obvious change in the microstrain was observed when the heat treatment temperature rose from 140 to 200 °C. All of the crystalline samples had a microstrain value of ~0.11%. This fact rules out the possibility that the microstrain causes the conductivity change during the heat treatment. An increase in the crystallite size from 80 to 120 nm was observed when the heat treatment temperature was increased from 140 to 200 °C. The heat treatment alters the crystallite size and consequently leads to the change in surface area. Thus, the positive correlation of ionic conductivity with surface area directly indicates that surface conduction is the main contributor to the anomalous high ionic conductivity of the nanoporous β-Li_3PS_4.

The formation of the nanoporous structure during the dissociation of THF generates a large number of lattice defects and microstrain. While the microstrain exists in the entire sample, the defects are concentrated on the surface of the nanoporous β-Li_3PS_4. The defects cause a charge imbalance and create a space charge at the surface.[17] The space-charge region exhibits enhanced lithium vacancy conductivity.[3,18] The nanoporous β-Li_3PS_4 has a high surface-to-bulk ratio, and therefore, surface conduction is dominant in the overall conduction.[5,19] This fact also explains why the activation energy of the nanoporous β-Li_3PS_4 is significantly lower than that of the bulk β-Li_3PS_4.

The excellent conductivity of nanoporous β-Li_3PS_4 does not compromise its chemical and electrochemical stability. As expected, the nanoporous β-Li_3PS_4 has a broad electrochemical window. Figure 5a shows the cyclic voltammogram (CV) of a Li/β-Li_3PS_4/Pt cell, in which Li and Pt serve as the reference/counter and working electrodes, respectively. The potential was scanned from −0.2 to 5.0 V vs Li/Li$^+$ at a scan rate of 100 mV s^{-1}. The cathodic current corresponding to lithium deposition started just below 0 V, indicating excellent compatibility with lithium metal. The anodic current ascribed to lithium dissolution showed a peak from 0 to 0.22 V. No significant current was observed in the potential range of 0.22−5 V, as shown in Figure S5 with 10× amplification of the CV current scale. Thus, no side reactions occurred in the CV. The

dx.doi.org/10.1021/ja3110895 | J. Am. Chem. Soc. 2013, 135, 975−978

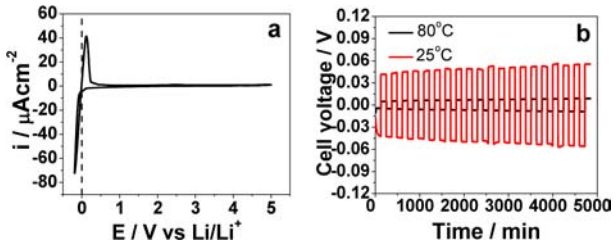

Figure 5. Electrochemical stability of β-Li_3PS_4 and cycling stability with metallic lithium electrodes. (a) CV of a Li/β-Li_3PS_4/Pt cell, where Li and Pt serve as the reference/counter and working electrodes, respectively. (b) Lithium cyclability in a symmetric Li/β-Li_3PS_4/Li cell. The cell was cycled at a current density of 0.1 mA cm^{-2} at room temperature and 80 °C.

nanoporous β-Li_3PS_4 is completely compatible with the lithium electrode up to 5 V, unlike the recently discovered $Li_{10}GeP_2S_{12}$,[2] in which the Ge substitution in the lithium thiophosphate compromises the chemical compatibility with metallic lithium.[9]

A symmetric Li/β-Li_3PS_4/Li cell was configured to demonstrate the cyclability and long-term compatibility of nanoporous β-Li_3PS_4 with metallic lithium.[20] Figure 5b shows the voltage profile of the cell cycled at room temperature and 80 °C. At room temperature, the cell presented a voltage of 41.6 mV at a current density of 0.1 mA cm^{-2}. The direct-current (dc) conductivity derived from the symmetric cell was 1.5×10^{-4} S cm^{-1}, which is very close to the alternating-current (ac) conductivity of 1.6×10^{-4} S cm^{-1} obtained from electrochemical impedance spectroscopy measurements. Negligible interfacial resistance between the lithium electrode and the solid electrolyte was observed, further confirming that the nanoporous β-Li_3PS_4 is completely compatible with metallic lithium. The cell showed excellent cyclability at room temperature and 80 °C (Figure 5b).

In summary, the nanoporous structure enhances the ionic conductivity of Li_3PS_4 by 3 orders of magnitude. Such a porous structure stabilizes the preferred metastable phase and provides a significant surface conduction mechanism. The results will inspire the pursuit of desirable physical properties through revisiting known materials at the nanoscale. Reducing the dimensions of materials leads to very different results, even in contrast to the prevailing view.[21,22]

■ ASSOCIATED CONTENT

Ⓢ Supporting Information

Experimental details and additional figures. This material is available free of charge via the Internet at http://pubs.acs.org.

■ AUTHOR INFORMATION

Corresponding Author

liangcn@ornl.gov

Notes

The authors declare no competing financial interest.

■ ACKNOWLEDGMENTS

This work was sponsored by the Division of Materials Sciences and Engineering, Office of Basic Energy Sciences, U.S. Department of Energy (DOE). The synthesis and characterization of materials were conducted at the Center for Nanophase Materials Sciences at Oak Ridge National Laboratory, which is sponsored by the Division of Scientific User Facilities, U.S. DOE.

■ REFERENCES

(1) Makiura, R.; Yonemura, T.; Yamada, T.; Yamauchi, M.; Ikeda, R.; Kitagawa, H.; Kato, K.; Takata, M. *Nat. Mater.* **2009**, *8*, 476.
(2) Kamaya, N.; Homma, K.; Yamakawa, Y.; Hirayama, M.; Kanno, R.; Yonemura, M.; Kamiyama, T.; Kato, Y.; Hama, S.; Kawamoto, K.; Mitsui, A. *Nat. Mater.* **2011**, *10*, 682.
(3) Maier, J. *Nat. Mater.* **2005**, *4*, 805.
(4) Homma, K.; Yonemura, M.; Kobayashi, T.; Nagao, M.; Hirayama, M.; Kanno, R. *Solid State Ionics* **2011**, *182*, 53.
(5) Puin, W.; Rodewald, S.; Ramlau, R.; Heitjans, P.; Maier, J. *Solid State Ionics* **2000**, *131*, 159.
(6) Saito, Y.; Maier, J. *J. Electrochem. Soc.* **1995**, *142*, 3078.
(7) Arico, A. S.; Bruce, P.; Scrosati, B.; Tarascon, J. M.; Van Schalkwijk, W. *Nat. Mater.* **2005**, *4*, 366.
(8) Mizuno, F.; Hayashi, A.; Tadanaga, K.; Tatsumisago, M. *Adv. Mater.* **2005**, *17*, 918.
(9) Mo, Y.; Ong, S. P.; Ceder, G. *Chem. Mater.* **2012**, *24*, 15.
(10) Tachez, M.; Malugani, J. P.; Mercier, R.; Robert, G. *Solid State Ionics* **1984**, *14*, 181.
(11) Mercier, R.; Malugani, J. P.; Fahys, B.; Robert, G.; Douglade, J. *Acta Crystallogr., Sect. B* **1982**, *38*, 1887.
(12) Machida, N.; Yamamoto, H.; Asano, S.; Shigematsu, T. *Solid State Ionics* **2005**, *176*, 473.
(13) Cadioli, B.; Gallinella, E.; Coulombeau, C.; Jobic, H.; Berthier, G. *J. Phys. Chem.* **1993**, *97*, 7844.
(14) Rey, J. F. Q.; Ferreira, F. F.; Muccillo, E. N. S. *Solid State Ionics* **2008**, *179*, 1029.
(15) Guo, Y. G.; Lee, J. S.; Maier, J. *Adv. Mater.* **2005**, *17*, 2815.
(16) Liang, C.; Terabe, K.; Hasegawa, T.; Aono, M.; Iyi, N. *J. Appl. Phys.* **2007**, *102*, No. 124308.
(17) Maier, J. *Z. Phys. Chem.* **2003**, *217*, 415.
(18) Maier, J. *Prog. Solid State Chem.* **1995**, *23*, 171.
(19) Maier, J. *Solid State Ionics* **2004**, *175*, 7.
(20) Burns, J. C.; Krause, L. J.; Le, D.-B.; Jensen, L. D.; Smith, A. J.; Xiong, D.; Dahn, J. R. *J. Electrochem. Soc.* **2011**, *158*, A1417.
(21) Heitjans, P.; Indris, S. *J. Phys.: Condens. Matter* **2003**, *15*, R1257.
(22) Gadjourova, Z.; Andreev, Y. G.; Tunstall, D. P.; Bruce, P. G. *Nature* **2001**, *412*, 520.